**Egyptian Journal of Chemistry**

**http://ejchem.journals.ekb.eg/**

# Fabrication, Characterization, And Monitoring Of The Propagation Of Nanocrystalline Zno Thin Film On Ito Substrate Using Electrodeposition Technique

**E. M. Elsayed [1], Ashraf K Eessaa [2], M. M. Rashad [1], S. M. Abdelbasir [1], A. M El-Shamy [3,*]**

[1] *Central Metallurgical Research and Development Institute, P.O Box 87 Helwan, Cairo, Egypt*

[2] *Nanotechnology central lab, Electronics Research Institute (ERI), Cairo, Egypt*

[3,*] *National Research Centre, Physical Chemistry Department, Electrochemistry and Corrosion Lab., El-Bohouth St. 33, Dokki, P.O. 12622, Giza*

**Abstract**

At varying temperatures ranging from 25 $^0$C to 75 $^0$C, nanocrystalline zinc oxide ZnO films were customized onto indium doped tin oxide (ITO) substrates based on aqueous solutions of zinc nitrate. The electrodeposition technique was used to achieve this procedure. To grasp the deposition strategy, linear sweep voltammetry and chronopotentiometry procedures were completed, and the effects of different factors were evaluated and discussed. Temperature and current have a significant influence on the development of ZnO films. According to the model developed by Scharifker and Hills, the mechanism of nucleation altered with the potential, and it was discovered to be instantaneous at potentials between -800 and -1200 mV. At voltages greater than -1400 mV, the method of development was non-instantaneous and gradual. Following the X-ray profiles, the production of the Zincite phase with a crystallite size of 61 nm was confirmed, and the films that were created were smooth and compact

**Keywords:** Zinc oxide; Electrodeposition; ITO; Chronoamperometry; Linear sweep voltammetry (LSV); Battery energy storage.

## 1. Introduction

Because of their size-dependent characteristics and a broad range of applications, nanocrystalline semiconducting materials have attracted a great deal of attention [1-3]. Zinc oxide (ZnO) is a semiconducting material with a bandgap energy of 3.37 eV and is one of the most exciting materials to study. It is regarded as a promising material for applications such as solar cells, sensors, piezoelectric transducers, photocatalysts, electroluminescent devices, and laser diodes [4, 5]. In a variety of technological and industrial domains, such as catalysis [6-8], acoustic wave devices [9, 10], an n-type layer in solar cells [11, 12], sensors, battery energy storage, and many more sophisticated applications [13–15], zinc oxide thin films are utilized. A variety of processes, including pulsed laser deposition [16], Sol-gel [17], and electrochemical deposition [18–20], may be used to create zinc oxide films. Comparing electrochemical preparation of ZnO to other techniques [21–23], electrochemical preparation is more advantageous. From the standpoint of the environment, electrochemistry is a straightforward, environmentally friendly, and cost-effective method. Also advantageous is that the thickness of the resulting film can be readily controlled, and the processing may be carried out at low temperatures [24-26]. Several investigations on the electrolytic synthesis of ZnO have been conducted, employing both non-aqueous [27-29] and aqueous electrolytes [30]. Traditionally, electrodeposition from an aqueous solution was accomplished by utilizing a zinc chloride or zinc nitrate bath as a starting point. Regardless of the scenario, it has been discovered that the solution composition is crucial for controlling the shape and structure of the deposited zinc oxide [31-33]. While non-aqueous baths, such as DMSO (diphenyl sulfoxide), form deposits at greater operating temperatures than aqueous media, they do so without the generation of zinc hydroxide in the electrolyte [34-35], which is a significant advantage [36]. It is possible to regulate the development of zinc oxide grains even when the electrodeposition temperature is kept below 100 $^0$C. This allows the growth of zinc oxide grains to form nanocolumnar, sheets, and unoriented polycrystalline films. If you

*Corresponding author e-mail: elshamy10@yahoo.com

Receive Date: 08 March 2022, Revise Date: 12 May 2022, Accept Date: 18 May 2022

DOI: 10.21608/EJCHEM.2022.126134.5595

compare the electrochemical deposition of zinc oxide films from a nitrate bath to an organic (alcoholic) bath, the electrochemical deposition of zinc oxide films from a nitrate bath is more advantageous since it is simpler and more cost-effective [37-39]. The usage of electrodes containing nanostructured zinc oxide has been mentioned as a potential trend for improving the efficiency of solar cells soon. Researchers have looked at the effects of zinc oxide content, bath temperature, and pH value on the formation of zinc oxide films using a variety of methodologies [40, 41]. The deposition of zinc oxide layers from a nitrate bath maintained at 335 $^{o}$C was shown and the change in hydroxyl ion concentration at the cathode was measured in many studies [42]. In this study, it was discovered that even a little alteration in the electrodeposition parameters might cause spectacular changes in the morphology and structure of the ZnO films. Thus, the purpose of this study was to investigate the electrodeposition of nanostructured ZnO layers using a zinc-nitrate bath and to discuss the effects of temperature, stirring, deposition time (including the amount of time spent stirring), electrode potential (including the amount of current used), and cathodic current density on the structural properties of the zinc oxide film [43].

## 2. Experimental Work

Using an indium doped tin oxide (ITO) sheet as the working electrodes, the electrodeposition experiments were carried out in a three-electrode cell, which was employed to conduct the tests. Silver/ silver chloride was employed as the counter electrode, and a platinum planner sheet with a surface area of 1 $cm^2$ was used as the reference electrode. It was decided to make the ITO working electrode of a conductive glass sheet with a resistance of 15 ohms/meter (Pilkington Group Ltd). Both the working and counter electrodes have an active surface area of (1 $cm^2$). The spacing between the ITO and Pt electrodes within the cell was kept constant at 0.4 cm throughout the experiment. The reference electrode was made of silver/silver chloride (Ag/AgCl) and was linked to the rest of the circuit via a salt bridge. The electrodeposition bath comprised an analytical grade of 0.1 M $Zn(NO_3)_2$ +0.05M $KNO_3$ dissolved in deionized water, which was used for the electrodeposition process [44]. An electronic thermostat was used to measure the temperature of the electrolyte between 0 and 75 $^{o}$C. Except for a small experiment in which the nitrate baths were continually agitated using a magnetic stirrer, the electrolytes were kept static. Before ZnO film deposition, the ITO conductive electrodes are washed and sonicated in an isopropanol solution for 5 minutes to remove any remaining contaminants. After that, the deposited films are washed with acetone to remove any remaining residue. Voltammetric studies were conducted by sweeping the electrode potential from 0 to -2000 mV at a constant scan rate of 10 mV/s for the whole duration of the experiment. These voltammetric investigations were carried out and recorded with the use of a Volta lab Model 21 PGP Potentiostate/Galvanostate (PGP for short). A 45-minute annealing procedure at 500 $^{o}$C followed the electrodeposition process. After being rinsed with water and ethyl alcohol, the films were dried. The X-ray diffraction data of the deposited ZnO films were obtained using a Shimadzu XD-D1 X-ray diffractometer with Cu K radiation (= 1.5405 $A^0$), which was used to generate the data. The morphology of the film surface was studied using a scanning electron microscope (SEM) operating at a speeding voltage of 20 kV, as described before (HITACHI, S-4700 Y) [45].

## 3. Results and discussion

### 3.1. Cyclic voltammetry

The cyclic voltammogram recorded with an ITO substrate in a bath containing 0.1 M $KNO_3$ and 0.1 M $KNO_3$+0.05 M $Zn(NO_3)_2$ is shown in Fig. 1. The baths used were 0.1 M $KNO_3$ and 0.1 M $KNO_3$+0.05 M $Zn(NO_3)_2$. As can be seen in Fig.1a, the electrodeposition of nitrate ions from a solution containing these ions is related to the formation of a cyclic voltammetric curve. When using cyclic voltammetry, the current of the deposition begins at a potential of -1V. A step increase in deposition current follows afterward, reaching up to 15 mA/$cm^2$ in response to the cathodic reduction of $NO_3^-$ ions at potential -1.2V [46], which is consistent with cathodic reduction. On anodizing the scan, the recorded current behavior is related to the development of oxygen, which is reversed in the scan direction. Except as otherwise specified in this section, the cyclic voltammogram shown in Fig. 1b is performed under the same circumstances as previously stated in the presence of 0.1 M $Zn(NO_3)_2$. In this case, the cyclic voltammetric curves behave in a manner like that previously shown in Fig.1a (with $KNO_3$). The electrodeposition of $Zn^{2+}$ ions is necessitated by the presence of nitrate ions in the electrolyte throughout the process. This is owing to the possibility that a minor current may be seen in the $KNO_3$ bath within the current and potential ranges that have been investigated. Fig. 1b shows that the peak of zinc metal dissolution (anodic oxidation) has gone in 0.05 M $KNO_3$ solution, suggesting that the deposited film is composed entirely of pure ZnO phase and that no zinc metal deposition has occurred (Fig.1b). Furthermore, Fig.1b demonstrated that the deposition potential window for the ZnO preparation was between -1 and -1.3V for the ZnO preparation. Sodium nitrate ions serve as an oxygen precursor

source, and the presence of these ions is required for the deposition of zinc oxide from the nitrate bath [47]. Eq. (1) predicts that the cathodic deposition of zinc oxide will occur during the electro-reduction of 0.05 M KNO3 [Eq. (1)]. In the next step, the OH- ions from equation (1) mix with Zn2+ ions to form zinc hydroxide ($Zn(OH)_2$), as illustrated in Eq. (2). $Zn(OH)_2$ is formed as a consequence, which dissociates to form ZnO film [Eq. (3)] [48].

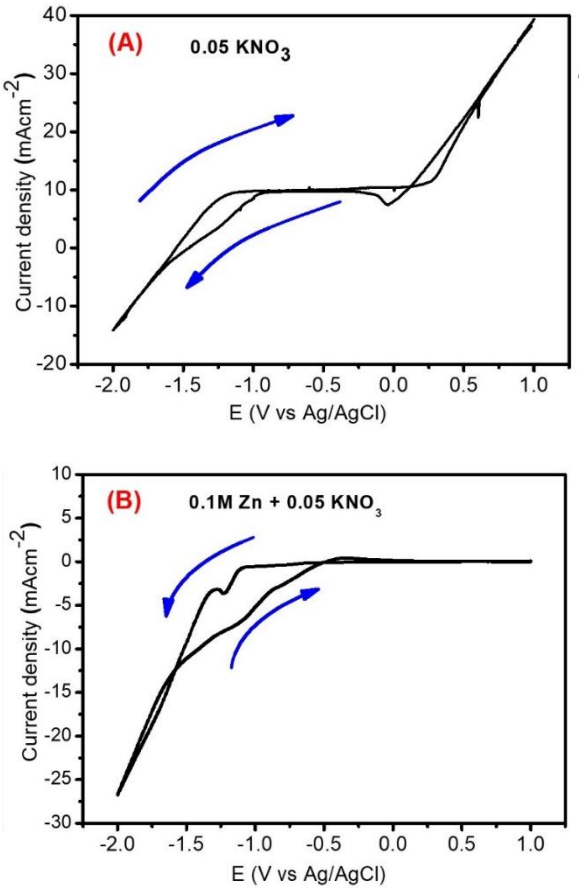


**Fig. 1.** Cyclic voltametric curves recorded with ITO electrode in bath containing (a) 0.05 M $KNO_3$ (b) 0.05 M $KNO_3$ + 0.1 M Zn $(NO_3)_2$. (Electrolyte temperature: $25^0$C; rate of scan= 10 mV $s^{-1}$; rate of stirring= 0 rpm).

$$NO_3^- + H_2O + 2\ e^- = NO_2^- + 2\ OH^- \quad (1)$$
($E_0$ = - 0.24 V vs. SCE)

$$Zn^{2+} + 2\ OH^- = Zn(OH)_{2\,(S)} \quad (2)$$

$$Zn(OH)_{2\,(S)} = ZnO + H_2O \quad (3)$$

The reaction net result is:

$$Zn^{2+} + NO_3^- + 2\ e^- = ZnO + NO_2^- \quad (E_0 = -0.246\ V\ vs.\ SCE) \quad (4)$$

Fig. 2 depicts results obtained by measuring the cyclic voltammograms seen at stirring rates of 0, 500, 1000, and 1500 rpm in a bath containing 0.1 M $KNO_3$ and 0.1 M $Zn(NO_3)_2$ at various stirring rates. With rising rates of stirring from 0 to 1500 rpm, the measured current of deposition increases in its negative values, and this trend continues. Increasing the rate of stirring results in a reduction in the thickness of the layer next to the cathode and a shortening of the route of the dispersed ions toward cathodic deposition, as well as a reduction in the thickness of the layer adjacent to the cathode [49]. When zinc nitrate solution is electrolytically depleted, zinc oxide films are formed because of the sluggish transfer of charges between concentrated solutions [50]. A poor and exposed ITO cathode is produced when the rate of agitation is increased from zero to five hundred revolutions per minute (rpm) (Fig. 1). The film is also broken and less compact when the stirring speed is increased to 1000 rpm, which is achieved by raising the stirring rate. A further increase in the rate of stirring to 1500 rpm results in a significant rise in the amount of damage to the deposited coating. Even though the current density increased as the stirring rate increased, the results revealed that poor quality and non-compacted ZnO layers were related to stirring rates of 500, 1000, and 1500 rpm. While the deposited film produced by a stationary solution (0 rpm) is very compact, homogeneous, and completely covers the substrate, the film produced by a moving solution (0 rpm) is not formed. As a result, when it comes to creating high-quality ZnO films, the synthesis of ZnO films with stationary electrolytes is preferred [51].

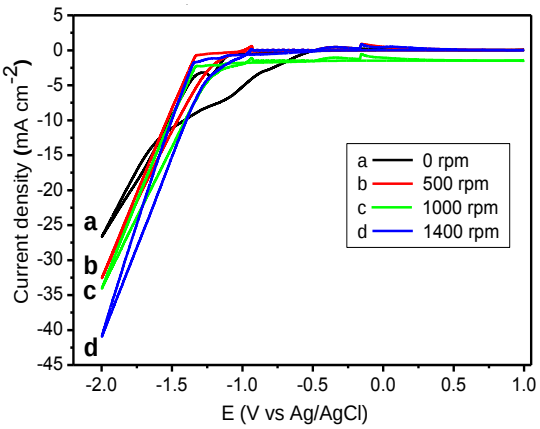


**Fig. 2.** Cyclic voltammograms recorded with ITO electrode in bath containing 0.05 M $KNO_3$ + 0.1M $Zn(NO_3)_2$ using various rate of agitation (Bath temperature:$25^0$C; rate of scan = 10 mV/s).

### 3.2. Linear sweep voltammetry

#### 3.2.1. Influence of operating temperature

Fig. 3 depicts the linear sweep voltammetry (LSV) curves acquired for ZnO deposition on an ITO cathode during the experiment, as well as the results of the experiment. The graphic depicts the variation in current and potential as a function of electrolyte temperature. The current density increases as the electrolyte temperature rise, reaching a maximum value of 38 mA $cm^{-2}$ at 75 $^0$C, which is a significant increase from the initial value. With a negative potential of 1.25 mV at 25 $^0$C, the potential of deposition changes to a positive potential of 0.97 V when the temperature is raised to 75 $^0$C. More importantly, when the same applied potential is used, the current increases gradually as the temperature rises with increasing temperature. Electrodeposition of ZnO films is difficult when the cathode potential is larger than -1.28 V and the temperature is less than 0 $^0$C [52]. While the rate of deposition is growing, the increase is occurring at a snail's pace. In response to increasing the electrolyte temperature, the number of dislocation lines per unit area of layer (in this case the ZnO layer) was reduced, as was the tension between layers. Previously, the microstructure of the ZnO film that had been created had been investigated, and it was observed that it seemed to be dependent on the temperature of the electrolyte [53]. The temperature influences the thickness of the film as well, and it has been determined that in this research, electrodeposition of ZnO film should be carried out at a high electrolyte temperature (75 $^0$C) [54].

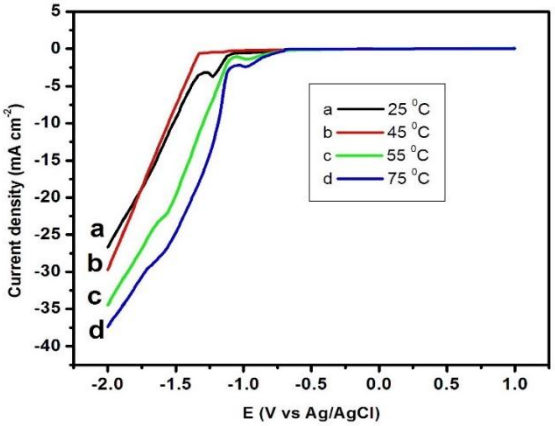


**Fig. 3.** LSV curves recorded in bath containing 0.05 M $KNO_3$ + 0.1 M Zn $(NO_3)_2$ at various electrolyte temperatures rate of scan = 10 mV $s^{-1}$; rate of stirring = 0 rpm.

#### 3.2.2. Chronopotentiomtric behavior

During the electrodeposition of ZnO layers in a solution with 0.05 M $KNO_3$ and 0.1 M $Zn(NO_3)_2$ concentrations, chronopotentiometry curves were produced. These are shown in Fig. 4. To determine the most appropriate current density for the deposition process, as well as the deposition rate at various current densities (such as 1, 2, 5, 1, 10, 20, 30, and 40 mA.$cm^{-2}$), the electrodeposition procedure was carried out at a variety of current densities (such as -1, -2, 5, 1, 10, 20, and 30 mA.$cm^{-2}$) including -1, 2, 5, 1, 10, 20, and 30 mA.$cm^{-2}$. Starting with the electrodeposition current, the potential quickly rises to the value that was previously measured. This is followed by a fast fall in the potential value until it is reached at its steady-state potential value. It is possible to deduce that the electrode surface is being covered by the ZnO film layer at a faster rate because of the decrease in potential value. The electrodeposition potential rises to a certain value in response to the passage of time, then quickly increases to attain a steady-state, and then rapidly decreases again. This steady-state condition depicts the situation in which the deposited film completely covers the whole ITO surface of the substrate (cathode) [55].

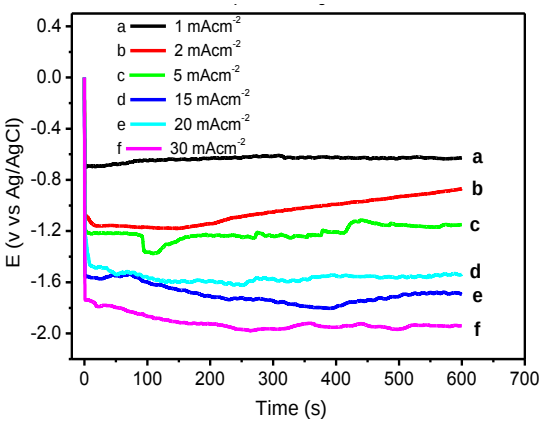


**Fig. 4**. Potential-time curves resulted at different current densities in a solution containing 0.05 M $KNO_3$ + 0.1 M Zn $(NO_3)_2$.

### 3.3. Chronoamperometric behavior

Fig. 5 shows the current time curves produced by using an ITO electrode in an electrolyte solution comprising 0.05 M $KNO_3$ and 0.1 M Zn $(NO_3)_2$ and an electrolyte solution containing 0.05 M $KNO_3$ and 0.1 M Zn $(NO_3)_2$. The current density data are quite comparable to the readings acquired during the first 70 seconds of the experiment. In the next seventy seconds, the behavior of the two systems diverges, with the density of cathodic current quickly rising after passing the applied potential. Crystal nucleation begins, and as a result, the current density of ZnO deposition rises quickly, and the development of each crystal nucleus results in an increase in the effective area of the ITO cathode. Additional proof for this is provided by the developments in three-dimensional nucleation and crystallization shown by the current

study [56]. Fig. 5 indicates that as the applied potentials are elevated to greater levels, the observed current densities increase (Fig. 5a-f). This is probably due to the existence of a higher density of deposited films than is typical in this environment. An increase in deposition duration of more than 70 seconds leads to an equalization of the value of the deposition current, which is followed by a plateau at the steady-state (constant) level of the current. To observe the behavior of the electrochemical nucleation process, it is necessary to apply an electrode potential to it; the current density value seems to be the same in both circumstances. That the ZnO layer has entirely occupied the ITO cathode is shown by the presence of this layer [57]. The measured currents are maintained at the following constant values:

The following values were obtained: – 0.5 mA cm2 at potential -0.8 V (curve a), – 1 mA cm-2 at potential -0.9 V (curve b), – 2 mA cm-2 at potential -1 V (curve c), – 5.9 mA cm-2 at potential -1.1 V (curve d), – 10 mA cm-2 at potential -1.2 V. Due to these considerations, the best conditions for ZnO electrodeposition from a nitrate bath are likely to be at an electrode potential of -1.2 V, a bath temperature of 75 $^{o}$C, and an electrolyte composition consisting of 0.1 M $Zn(NO_3)_2$ dispersed in 0.05 M $KNO_3$ with an unagitated solution, as illustrated in Figs. 1, 2, 3, and 4. Scharifker and Hills employed a constant potential technique to build a model that would illustrate the electro-crystallization and nucleation development that occurred over the preceding 10 seconds. Instantaneous or slow growth may be seen in the development of electro-nucleation progress, which can be divided into two categories. Within the initial few seconds following the creation of ZnO films, the influence of potential on their nucleation is seen in Fig. 6. Many research have shown that transient values may be estimated by comparing the recorded curves to a theoretical curve (or collection of curves) that has been provided for the development of electro-nucleation in three dimensions [58]. The idioms for both progressive nucleation and instantaneous nucleation were determined using Equations (5) and (6) in conjunction with each other.

$$I^2/i^2_{max} = 1.9542\ [t_{max}/t]\ \{1\text{-}\exp\ [-1.2564\ t/t_{max}\}^2 \quad (5)$$

$$I^2/i^2_{max} = 1.2254\ [t_{max}/t]\ \{1\text{-}\exp\ [-2.3367\ (t/t_{max})^2\}^2 \quad (6)$$

Where $t_{max}$ is the time of maximum current density $i_{max.}$

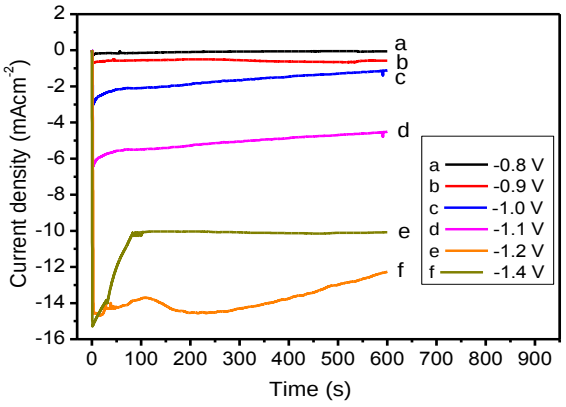


**Fig. 5.** Chronoamperometeric curves recorded at constant potentials in electrolyte containing 0.1 M Zn $(NO_3)_2$ + 0.05 M $KNO_3$ (Bath temperature:75$^{0}$C; rate of stirring = 0 rpm).

Illustration of the similarities between theoretical and real experimental curves that have been observed in the previous section. When the theoretical and experimental curves for the electrodeposited film were compared, it was possible to detect when the ZnO layer nucleated.

At lower potentials of -0.8 and -1.2 V, the nucleation process for the ZnO layer mirrored the instantaneous behavior seen at higher potentials (Figs. 6a,b). It demonstrated a progressive process within the nucleation zone when the negative potential of -1.4 V was applied, as shown in Fig. 6c (on the other hand). According to the results, when the potential was as low as -1.2V, nuclei at active ITO sites grew according to the instantaneous mechanism, and when the potential was as high as -1.4V, nuclei at active ITO sites expanded according to the progressive method [59].

### 3.4. Thickness measurements

The variations in film thickness as a function of the deposition potential are shown in Fig. 7. The weight difference technique [60–62] was used to determine the thickness of the film. In this study, it was discovered that raising the voltage of the cathode to -1.2 V is followed by a significant rise in the film thickness, with the greatest thickness recorded at 8000 nm using an ITO substrate. A further rise in cathode potential over -1.2 V, on the other hand, leads to a reduction in the thickness of the film. This may be caused by the chance that the formed film is dissolved in an acidic nitrate bath at potentials between -1.3 and -1.4 V [63, 64], which is a possibility. Finally, it seems that the electrochemical production of ZnO films from a nitrate bath

containing 0.1 M $Zn(NO_3)_2$ in 0.05 M $KNO_3$ should be carried out at an electrode potential of -1.2V under non-stirred circumstances to get the best results. In addition, the temperature of the bath should be kept at 75 $^oC$ [65].

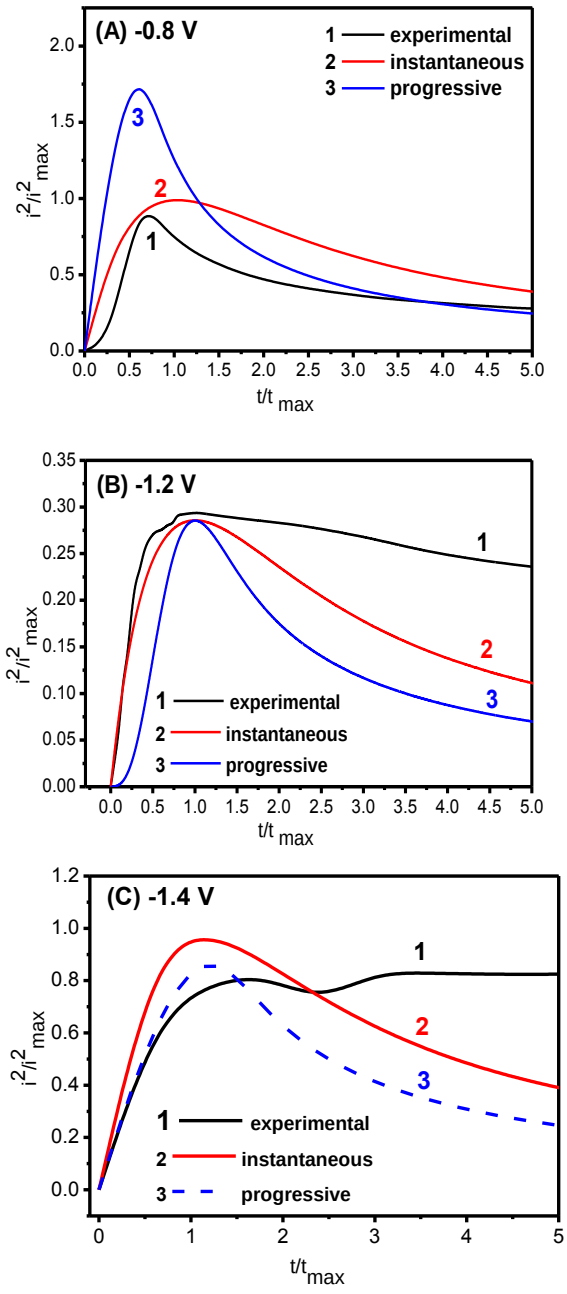


**Fig. 6**. Plot of $i^2/i^2_{max}$ versus $t/t_{max}$ plots recorded with zinc oxide layer deposited from 0.1M$ZnNO_3$ + 0.05M $KNO_3$ at potential (a)-0.8 V, (b)-1.2 V, and (c)-1.4 V for 10 min. (Stirring rate= 0 rpm and temperature: 75 $^0C$).

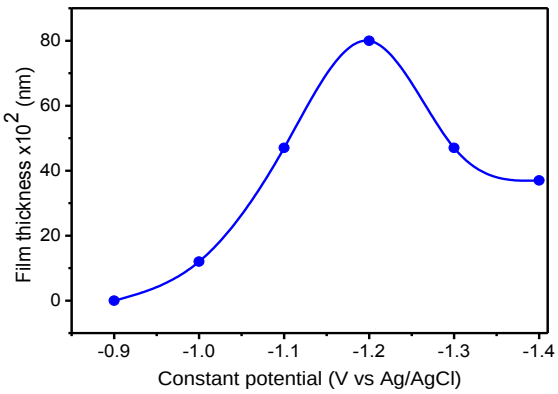


**Fig. 7.** Variation in thickness of film with electrode potential in solution containing 0.1M $Zn(NO_3)_2$ + 0.05M $KNO_3$ for 100 min (Bath temperature = 75$^0C$; rate of stirring = 0 rpm).

### 3.5. Optical properties

Figs. 8a,b show the percentage of the transmittance spectrum and the bandgap energy of the electrodeposited ZnO film, respectively, for the electrodeposited ZnO film (Figs. 8b). The charge transfer process from the valence band to the conduction band of ZnO is responsible for the appearance of an edge at a wavelength of around 400 nanometers. The presence of blue shifts between the wavelengths of 290 and 300 nanometers has been observed, as well. Because the bandgap value of the ZnO film generated is less than the bandgap value of the bulk ZnO, the film has a lower bandgap value than the bulk ZnO film created (3.37 eV). A shortening of both the valance and conduction bands, which resulted in a modification of the band structure, may be the explanation for this, according to the band structure [66].

### 3.6. Structure analysis.

On the right side of Fig. 9, you can see the x-ray diffractogram of the ZnO film that was formed by depositing it from a nitrate bath at a potential 1.2 V on an ITO cathode for 10 minutes at 75 $^oC$ and then heating it to 400 $^oC$ for 60 minutes in the open air. It can be seen in the photo that the ZnO thin layer that was generated is a pure fine single phase with no existing impurities, as can be shown in Fig. 9. It also shows other properties, such as the distinctive peaks of (Zincite) in a hexagonal pattern that are characteristic of the mineral [JCPDS 01-079-0207] [JCPDS 01-079-0207]. Two Zincite diffraction peaks have been discovered, at the coordinates of 31.65, 34.26, 36.11, 47.34, 51.48, 56.38, 62.81, 67.74, and 69.23 [67]. These coordinates correspond to the crystal planes (100), (002), (101), (201), and (110), which are corresponding to the crystal planes (100), (002), (101), and (110) [JCPDS 01-079-0207] [JCPDS 01-079-0207].

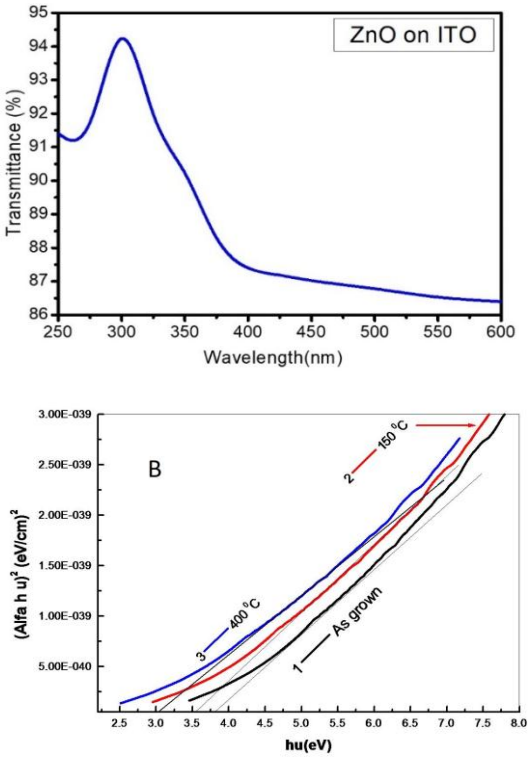


**Fig. 8.** (A)Transmittance spectra of ZnO and (B) Band gap of ZnO electrodeposited film. (ITO cathode, Pt anode, no stirring, Annealing time=60 min, 0.1M $Zn(NO_3)_2$ + 0.05M $KNO_3$-E= -1.2V for 100 min, bath temp = 75 $^0$C).

The peaks of the film as they have been created are crisp, and they suggest that the crystalline planes are in a strong state of condition. A computer program was used to determine the size of the crystallite using the Scherer equation and the primary diffraction peaks [68], which were then manually recorded. The crystal's diameter was measured to be 61 nm in diameter.

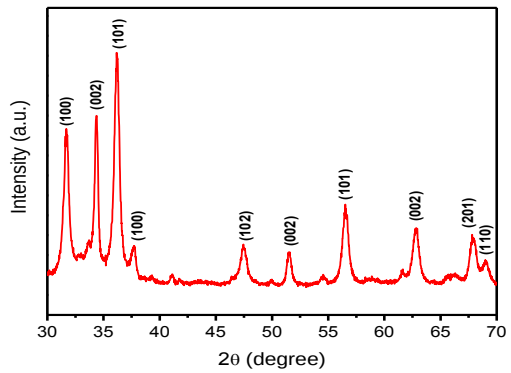


4. Fig. 9. X-Ray Diffraction peaks for ZnO film deposited at -1.2V and annealing at 400 $^0$C for 60 minutes (Electrolysis conditions: 75 $^0$C, stirring rate = 0 rpm, time=10 min, ITO, 0.1M $Zn(NO_3)_2$+ 0.1M $KNO_3$).

### 3.7. Surface morphology

As shown in Fig. 10, there is a direct link between the geometry of as-deposited zinc oxide films and their electrode potential. It is under these conditions that the films were electrodeposited for a total of 5 minutes using chronoamperometric settings of -0.8 and -1.2 V for a total of 5 minutes. In Fig. 10, the scanning electron micrographs of a film, which was deposited at a constant potential of -0.8 V, are shown in the first row. Images of a film that was deposited at an applied constant potential of -0.8 V are shown in Fig. 10b by scanning electron microscopy [69]. On the ITO surface, which is only partially covered by the film, aggregated particles with a semispherical structure can be seen forming aggregates. Fig. 10b shows micrographs of the zinc oxide layer electrodeposited at -1.2 V, as an illustration of this. Compared to Fig. 10a, which shows the identical film electrodeposited at +1.2 V, the film in Fig. 10b seems to be more adherent, smooth, and has fully covered the whole surface area of the ITO electrode. Increasing the applied potential of the deposited layer from -1 to -1.2 V results in a significant increase in the grain size, as can be shown [70].

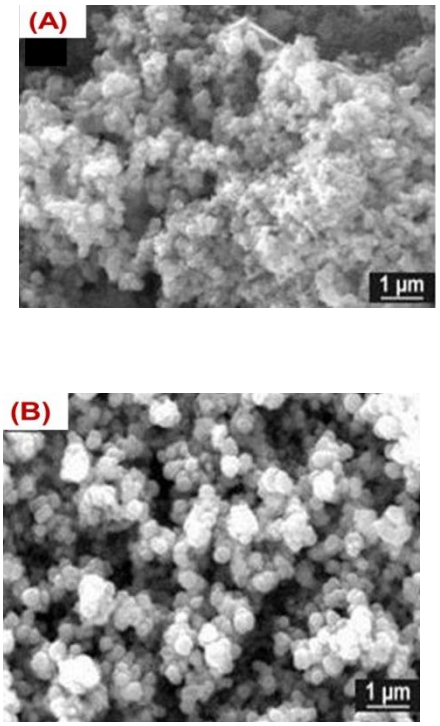


**Fig. 10.** Scanning electron micrographs for Zinc Oxide films electrodeposited at the potential: (a) -0.8 V, and (b) –1.2 V.

## 4. Conclusions

A zinc nitrate bath was used to electrochemically deposit zinc oxide coatings on an ITO substrate in this investigation, and this was done on purpose to get the desired results. Electrodeposition processes have been monitored using techniques such as cyclic voltammetry, chronoamperometry, chronopotentiometry, and laser scanning voltammetry (LSV). The analysis and optimization of electrochemical parameters such as electrode potential, deposition length, bath temperature, and rate of bath agitation were carried out in this research. In conclusion, it was discovered that the optimal conditions for electrodeposition parameters were -1.2 V, 75 0C, and a non-stirred solution for a total of 10 minutes. Within the first few seconds of the experiment, the process of ZnO nucleation (as predicted by the Scharifker and Hills model) showed quick activity at low electrode potentials, indicating that it was active within the first few seconds (-0.8 and -1.2 V). It was observed that nucleation formation was both slow and quick at potentials larger than -1.4 V. In the experiment, the bandgap energy value of the electrodeposited zinc oxide layer was determined to be 3.5 eV, according to the results. The hexagonal Zincite structure with a crystallite size of 61 nm was identified via the process of structural characterization and characterization of minerals. Using the constant potential approach (chronoamperometric imaging), scanning electron micrographs of the deposited layer were obtained, and smooth, compact, and aggregated particles were seen spreading entirely over the surface of the ITO cathode.

## Conflict of Interest

No conflict of interest is to be announced.

## Formatting of funding sources

Not applicable

## Acknowledgments

Not applicable

## References

[1] A. Kathalingam, N. Ambika, M.R. Kim, J. Elanchezhiyan, Y.S. Chae, J.K. Rhee, Chemical bath deposition and characterization of nanocrystalline ZnO thin films, Mater. Sci. Pol. Vol. 28, No. 2 (2010).

[2] K. M. Zohdy, R. M. El-Sherif, S. Ramkumar, A. M. El-Shamy. Quantum and electrochemical studies of the hydrogen evolution findings in corrosion reactions of mild steel in acidic medium, Upstream Oil and Gas Technology 6, 100025 (2021). https://doi.org/10.1016/j.upstre.2020.100025

[3] Photovoltaic and Supercapacitor performance of SnSe nanoparticles prepared through co-precipitation method, Mohd Arif Dar, D Govindarajan, Khalid Mujasam Batoo, Muhammad Hadi, GN Dar, https://doi.org/10.1080/10667857.2021.1950887

[4] D.K. Hwang, M.S. Oh, J.H. Lim, S.J. Park, ZnO thin films and light-emitting diodes, J. Phys. D. Appl. Phys. 40, R387 (2007). doi:10.1088/0022-3727/40/22/R01.

[5] N. Izyumskaya, V. Avrutin, Ü. Özgür, Y.I. Alivov, H. Morkoç, Preparation and properties of ZnO and devices, Phys. Status Solidi Basic Res. 244, 1439–1450 (2007). doi:10.1002/pssb.200675101.

[6] M. Laurenti, V. Cauda, Porous Zinc Oxide Thin Films: Synthesis Approaches and Applications, Coatings. 8, 67 (2018). doi:10.3390/coatings8020067.

[7] H.Y. Huang, H.J. Chiang, C.Z. Wu, Y. Lin, Y.K. Shen, Analysis on characteristics of ZnO surface acoustic wave with and without micro-structures, Micromachines. 10, (2019). doi:10.3390/mi10070434.

[8] S. Hamrouni, M.S. AlKhalifah, M.S. El-Bana, S.K. Zobaidi, S. Belgacem, Deposition and characterization of spin-coated n-type ZnO thin film for potential window layer of solar cell, Appl. Phys. A Mater. Sci. Process. 124, 555 (2018). doi:10.1007/s00339-018-1980-z.

[9] I. Boukhoubza, M. Khenfouch, M. Achehboune, B. Mouthudi, I. Zorkani, A. Jorio, Dynamics of the etching effects on the optoelectronic properties of ZnO nanorods, in: J. Phys. Conf. Ser., Institute of Physics Publishing, p. 12010 (2018). doi:10.1088/1742-6596/1081/1/012010.

[10] Z. Yuan, E. Han, F. Meng, K. Zuo, Detection and Identification of Volatile Organic Compounds Based on Temperature-Modulated ZnO Sensors, IEEE Trans. Instrum. Meas. 69, 4533–4544 (2020). doi:10.1109/TIM.2019.2948413.

[11] Samar M. Mouneir, Ali M. El-Hagrassi, Ashraf M. El-Shamy. A Review on the Chemical Compositions of Natural Products and Their Role in Setting Current Trends and Future Goals Egypt. J. Chem. 65(5): 491-506 (2022). DOI: 10.21608/ejchem.2021.95577.4486

[12] Efficient, highly stable Zn2+ doped NiO nanoparticles with enhanced magnetic and supercapacitor applications, S Sivakumar, Nazir Ahmad Mala, Khalid Mujasam Batoo, Emad H Raslan, https://doi.org/10.1080/10667857.2021.1949527

[13] J. Jiang, J. Pi, J. Cai, The Advancing of Zinc Oxide Nanoparticles for Biomedical Applications, Bioinorg. Chem. Appl. 2018, (2018).

doi:10.1155/2018/1062562.
[14] F.C.C. Ling, Z. Wang, L. Ping Ho, M. Younas, W. Anwand, A. Wagner, S.C. Su, C.X. Shan, Defects in zinc oxide grown by pulsed laser deposition, Phys. B Condens. Matter. 480, 2–6 (2016). doi:10.1016/j.physb.2015.09.034.
[15] K. Harun, F. Hussain, A. Purwanto, B. Sahraoui, A. Zawadzka, A.A. Mohamad, Sol-gel synthesized ZnO for optoelectronics applications: A characterization review, Mater. Res. Express. 4, 122001 (2017). doi:10.1088/2053-1591/aa9e82.
[16] M. Skompska, K. Zarębska, Electrodeposition of ZnO nanorod arrays on transparent conducting substrates-a review, Electrochim. Acta. 127, 467–488 (2014). doi:10.1016/j.electacta.2014.02.049.
[17] N. Livinus Okoli, Effect of Dip Time on Electrodeposited Zinc Oxide Nanofilm, Am. J. Mater. Synth. Process. 3, 7 (2018). doi:10.11648/j.ajmsp.20180302.11.
[18] M. Pławecki, E. Rówiński, Ł. Mieszczak, M. Pławecki, E. Rówiński, Ł. Mieszczak, Zinc oxide/cuprous(I) oxide-based solar cells prepared by electrodeposition Zinc Oxide/Cuprous(I) Oxide-Based Solar Cells Prepared by Electrodeposition, Acta Phys. Pol. A. 130, 1144–1147 (2016). doi:10.12693/APhysPolA.130.1144.
[19] Y. Robin, M. Moret, S. Ruffenach, R.L. Aulombard, O. Briot, Influence of the growth rate on the morphology of electrodeposited zinc oxide, Superlattices Microstruct. 73, 281–289 (2014). doi:10.1016/j.spmi.2014.05.032.
[20] E.M. Elsayed, A.E. Shalan, M.M. Rashad, Preparation of ZnO nanoparticles using electrodeposition and co-precipitation techniques for dye-sensitized solar cells applications, J. Mater. Sci. Mater. Electron. 25, 3412–3419 (2014). doi:10.1007/s10854-014-2033-9.
[21] Amal M. Abdel-Karim, Ashraf M. El-Shamy, Y. Reda. Corrosion and Stress Corrosion Resistance of Al Zn Alloy 7075 by Nano-Polymeric Coatings, Journal of Bio- and Tribo-Corrosion 8:57 (2022). https://doi.org/10.1007/s40735-022-00656-2
[22] Design and fabrication of iron-doped nickel oxide-based flexible electrode for high-performance energy storage applications, Nazir Ahmad Mala, S Sivakumar, Khalid Mujasam Batoo, Muhammad Hadi, Inorganic Chemistry Communications, 131 108797 (2021).
[23] T. Marimuthu, N. Anandhan, R. Thangamuthu, Electrochemical synthesis of one-dimensional ZnO nanostructures on ZnO seed layer for DSSC applications, Appl. Surf. Sci. 428, 385–394 (2018). doi:10.1016/j.apsusc.2017.09.116.
[24] E. Salih, M. Mekawy, R.Y.A. Hassan, I.M. El-Sherbiny, Synthesis, characterization and electrochemical-sensor applications of zinc oxide/graphene oxide nanocomposite, J. Nanostructure Chem. 6, 137–144 (2016). doi:10.1007/s40097-016-0188-z.
[25] N.P. Klochko, G.S. Khrypunov, Y.O. Myagchenko, E.E. Melnychuk, V.R. Kopach, K.S. Klepikova, V.M. Lyubov, A. V. Kopach, Electrodeposited zinc oxide arrays with the moth-eye effect, Semiconductors. 48, 531–537 (2014). doi:10.1134/S1063782614040162.
[26] O. Lupan, T. Pauporté, L. Chow, B. Viana, F. Pellé, L.K. Ono, B. Roldan Cuenya, H. Heinrich, Effects of annealing on properties of ZnO thin films prepared by electrochemical deposition in chloride medium, Appl. Surf. Sci. 256, 1895–1907 (2010). doi:10.1016/j.apsusc.2009.10.032.
[27] G. Riveros, D. Ramírez, A. Tello, R. Schrebler, R. Henríquez, H. Gómez, Electrodeposition of ZnO from DMSO solution: Influence of anion nature and its concentration in the nucleation and growth mechanisms, J. Braz. Chem. Soc. 23, 505–512 (2012). doi:10.1590/S0103-50532012000300018.
[28] E.M. Elsayed, F.A. Harraz, A.E. Saba, Nanocrystalline zinc oxide thin films prepared by electrochemical technique for advanced applications, Int. J. Nanoparticles. 5, 136–148 (2012). doi:10.1504/IJNP.2012.046242.
[29] Z.H. Gu, T.Z. Fahidy, R. Hornsey, A. Nathan, A study of the electrochemical synthesis of ZnO thin films, Can. J. Chem. 75, 1439–1444 (1997). doi:10.1139/v97-173.
[30] S. Karuppuchamy, S. Ito, Cathodic electrodeposition of nanoporous ZnO thin films from new electrochemical bath and their photoinduced hydrophilic properties, Vacuum. 82, 547–550 (2008). doi:10.1016/j.vacuum.2007.06.002.
[31] Amal M. Abdel‑Karim, Ashraf M. El‑Shamy, A Review on Green Corrosion Inhibitors for Protection of Archaeological Metal Artifacts, Journal of Bio- and Tribo-Corrosion 8:35 (2022). https://doi.org/10.1007/s40735-022-00636-6
[32] Mala, N.A., Dar, M.A., Sivakumar, S. et al. Electrochemical supremacy of cobalt-doped nickel oxide and its supercapacitor applications with its mesoporous morphology. J Mater Sci: Mater Electron (2022). https://doi.org/10.1007/s10854-022-08130-y
[33] A. Drici, G. Djeteli, G. Tchangbedji, H. Derouiche, K. Jondo, K. Napo, J.C. Bernède, S. Ouro-Djobo, M. Gbagba, Structured ZnO thin films grown by chemical bath deposition for photovoltaic applications, Phys. Status Solidi Appl. Res. 201, 1528–1536 (2004). doi:10.1002/pssa.200306806.
[34] B.N. Illy, A.C. Cruickshank, S. Schumann, R. Da Campo, T.S. Jones, S. Heutz, M.A. McLachlan, D.W. McComb, D.J. Riley, M.P. Ryan, Electrodeposition of ZnO layers for

photovoltaic applications: Controlling film thickness and orientation, J. Mater. Chem. 21, 12949–12957 (2011). doi:10.1039/c1jm11225b.
[35] T. MD, Doped Zinc Oxide Nanostructures for Photovoltaic Solar Cells Application, in: Zinc Oxide Based Nano Mater. Devices, IntechOpen, (2019). doi:10.5772/intechopen.86254.
[36] A.C. Cruickshank, S.E.R. Tay, B.N. Illy, R. Da Campo, S. Schumann, T.S. Jones, S. Heutz, M.A. McLachlan, D.W. McComb, D.J. Riley, M.P. Ryan, Electrodeposition of ZnO nanostructures on molecular thin films, Chem. Mater. 23, 3863–3870 (2011). doi:10.1021/cm200764h.
[37] S. Gupta, B. McDonald, S.B. Carrizosa, Surface Redox Chemistry of Immobilized Nanodiamond: Effects of Particle Size and Electrochemical Environment, J. Electron. Mater. 46, 4512–4526 (2017). doi:10.1007/s11664-017-5426-8.
[38] S. Otani, J. Katayama, H. Umemoto, M. Matsuoka, Effect of Bath Temperature on the Electrodeposition Mechanism of Zinc Oxide Film from Zinc Nitrate Solution, J. Electrochem. Soc. 153, C551 (2006). doi:10.1149/1.2205187.
[39] E.M. Elsayed, M.M. Rashad, M.R. Hussein, M.M.B. El-Sabbah, I.A. Ibrahim, Synthesis of Nanocrystalline Copper Ferrites by Electrochemical Techniques for Toxic Gas Sensing, Li Ion Battery and Medical Applications, Renew. Energy Sustain. Dev. 3, 267 (2017). doi:10.21622/resd.2017.03.3.267.
[40] M. Prestat, F. Vucko, B. Lescop, S. Rioual, F. Peltier, D. Thierry, Oxygen reduction at electrodeposited ZnO layers in alkaline solution, Electrochim. Acta. 218, 228–236 (2016). doi:10.1016/j.electacta.2016.09.050.
[41] A. M. El-Shamy, M. M. Abdel Bar. Ionic Liquid as Water Soluble and Potential Inhibitor for Corrosion and Microbial Corrosion for Iron Artifacts, Egypt. J. Chem. 64(4) 1867-876 (2021). DOI: 10.21608/ejchem.2021.43786.2887
[42] A. M. El-Shamy, (2020). A Review on: Biocidal Activity of Some Chemical Structures and Their Role in Mitigation of Microbial Corrosion, Egypt. J. Chem. 63(12), 5251-5267. DOI: 10.21608/ejchem.2020.32160.2683
[43] T. Pauporté, D. Lincot, Electrodeposition of semiconductors for optoelectronic devices: Results on zinc oxide, Electrochim. Acta. 45, 3345–3353 (2000). doi:10.1016/S0013-4686(00)00405-9.
[44] D. Pletcher, R. Greff, R. Peat, L.M. Peter, J. Robinson, Instrumental methods in electrochemistry, 1st editio, © Woodhead Publishing 2001, (2001). doi:10.1533/9781782420545.
[45] L. Heerman, E. Matthijs, S. Langerock, The concept of planar diffusion zones. Theory of the potentiostatic transient for multiple nucleation on active sites with diffusion-controlled growth, Electrochim. Acta. 47, 905–911 (2001). doi:10.1016/S0013-4686(01)00792-7.
[46] G. Barrera, F. Scaglione, M. Cialone, F. Celegato, M. Coïsson, P. Rizzi, P. Tiberto, Structural and Magnetic Properties of FePd Thin Film Synthesized by Electrodeposition Method, Materials (Basel). 13, 1454 (2020). doi:10.3390/ma13061454.
[47] Y. Kim, J. Jung, S. Kim, W.-S. Chae, Cyclic Voltammetric and Chronoamperometric Deposition of CdS, Mater. Trans. 54, 1467–1472 (2013). doi:10.2320/matertrans.M2013125.
[48] E.M. Elsayed, M.M. Rashad, I.A. Ibrahim, M.R. Hussein, M.M.B. El-Sabbah, Electrochemical synthesis of nanocrystalline NiFe2O4Thin film from aqueous sulphate bath, J. Alloys Compd. 798, 104–111 (2019). doi:10.1016/j.jallcom.2019.05.116.
[49] A. Saba, E. Elsayed, M. Moharam, M.M. Rashad, Electrochemical Synthesis of Nanocrystalline Ni 0.5 Zn 0.5 Fe 2 O 4 Thin Film from Aqueous Sulfate Bath, ISRN Nanotechnol. 2012, 1–8 (2012). doi:10.5402/2012/532168.
[50] S. Deki, H. Miki, M. Sakamoto, M. Mizuhata, Fabrication of Copper Ferrite Thin Films from Aqueous Solution by the Liquid-phase Deposition Method, Chem. Lett. 36, 518–519 (2007). doi:10.1246/cl.2007.518.
[51] M. F. Shehata, A. M. El-Shamy, K. M. Zohdy, E. S. M. Sherif, S. Z. El Abedin. Studies on the antibacterial influence of two ionic liquids and their corrosion inhibition performance, Appl. Sci. 10(4), 1444 (2020). https://doi.org/10.3390/app10041444
[52] El-Kattan, I. M., Khedr, M. H., Farghali, A. A., Elsaeidy, M., & Soliman, F. N. Single and combined impact of silica fumes with Functionalized multi-walled carbon Nanotubes and Nano silica on performance of cement mortars composites. In IOP Conference Series: Materials Science and Engineering 1046(1), 012024) (2021). IOP Publishing.
[53] E.M. Elsayed, M.M. Moharam, I. Ibrahim, H. Khalil, M.. Hussein, M. El-Sabbah, Electrochemical-Anodization Synthesis of Spinel Cobalt Ferrite Films on Various Substrates from Aqueous Medium, J. Basic. Appl. Chem. 8, 1–12 (2018). www.textroad.com (accessed April 26, (2021).
[54] M.M. Moharam, E.M. Elsayed, J.C. Nino, R.M. Abou-Shahba, M.M. Rashad, Potentiostatic deposition of Cu2O films as p-type transparent conductors at room temperature, Thin Solid Films. 616, 760–766 (2016).

doi:10.1016/j.tsf.2016.10.005.
[55] B.D. Cullity, S.R. Stock, Elements of X-ray Diffraction, Third Edit, Prentice-Hall, New York, 2001. https://www.scholars.northwestern.edu/en/publications/elements-of-x-ray-diffraction-third-edition (accessed April 26, (2021).
[56] E. M. Elsayed; Ashraf K. Eessaa; M. M. Rashad; Ashraf M. El-Shamy, Preparation and Characterization of ZnO Thin Film on Anodic $Al_2O_3$ as a Substrate for Several Applications, Egyptian Journal of Chemistry, Articles in Press, Accepted Manuscript, Available Online from 23 February (2022). DOI: 10.21608/ejchem.2022.110382.5021
[57] Y. Reda, H. M.Yehia, A. M.El-Shamy, Microstructural and mechanical properties of Al-Zn alloy 7075 during RRA and triple aging, Egyptian Journal of Petroleum 31 (2022) 9–13 https://doi.org/10.1016/j.ejpe.2021.12.001
[58] H. K. Farag, A. M. El-Shamy, E. M. Sherif, S. Z. El Abedin, Sonochemical Synthesis of Nanostructured ZnO/Ag Composites in an Ionic Liquid, Zeitschrift für Physikalische Chemie, 230 (12), 1733-1744 (2016). https://doi.org/10.1515/zpch-2016-0777
[59] Y. Reda, A. M. El-Shamy, Ashraf K. Eessaa, Effect of hydrogen embrittlement on the microstructures of electroplated steel alloy 4130, Ain Shams Engineering Journal 9(4), 2973-2982 (2018). https://doi.org/10.1016/j.asej.2018.08.004
[60] Y. Reda, K. M. Zohdy, A. K. Eessaa, A. M. El-Shamy, Effect of plating materials on the corrosion properties of steel alloy 4130, Egypt. J. Chem. 63(2), 579-597 (2020). DOI: 10.21608/ejchem.2019.11023.1706
[61] Y. Reda, A. M. El-Shamy, K. M. Zohdy, A. K. Eessaa. Instrument of chloride ions on the pitting corrosion of electroplated steel alloy 4130, Ain Shams Engineering Journal 11, 191–199 (2020). https://doi.org/10.1016/j.asej.2019.09.002
[62] M. F. Shehata, S. El-Shafey, N. A. Ammar, A. M. El-Shamy. Reduction of $Cu^{+2}$ and $Ni^{+2}$ ions from wastewater using mesoporous adsorbent: effect of treated wastewater on corrosion behavior of steel pipelines, Egypt. J. Chem. 62(9), 1587-1602 (2019). DOI: 10.21608/ejchem.2019.7967.1627
[63] El-Kattan, I. M., Tawfik, T. A., Metwally, K. A., Faried, A. S., & Zakid, W. Influence of nanosilica, metakaolin and Polypropylene Fiber on dynamic and physicomechanical properties of Portland cement mortar. In IOP Conference Series: Materials Science and Engineering 1046(1) 012002) (2021). IOP Publishing.
[64] A. M. El-Shamy, Ibrahim Abdelfattah, Ola I. Elshafie, M. F. Shehata. Potential removal of organic loads from petroleum wastewater and its effect on the corrosion behavior of municipal networks, J. Environ. Management, 219, 325-331 (2018). https://doi.org/10.1016/j.jenvman.2018.04.074
[65] El-Kattan, I. M., Farghali, A. A., Elsaeidy, M., Khedr, M. H., Soliman, F. N., & Emam, A. A. Dynamic and physio-mechanical effects of combined functionalised MWCNTs and nanosilica particles on cement composites. Advances in Cement Research, 34(1), 1-14 (2022).
[66] K. M. Zohdy, R. M. El-Sherif, A. M. El-Shamy, Corrosion and Passivation Behaviors of Tin in Aqueous Solutions of Different pH, Journal of Bio- and Tribo-Corrosion 7(2), 1-7 (2021). https://doi.org/10.1007/s40735-021-00515-6
[67] Ashraf K. Essa, A. M. El-Shamy and Y. Reda**,** Fabrication of Commercial Nano porous Alumina by Low Voltage Anodizing, Egypt. J. Chem. 61(1), 175-185 (2018). DOI: 10.21608/ejchem.2017.2189.1175
[68] A. M. El-Shamy, M. A. El-Hadek, A. E. Nassef, R. A. El-Bindary,. Optimization of the influencing variables on the corrosion property of steel alloy 4130 in 3.5 wt.% NaCl solution, Journal of Chemistry 2020, Article ID 9212491 (2020). https://doi.org/10.1155/2020/9212491
[69] M. A. Abbas, K. Zakaria, A. M. El-Shamy, S. Z. El Abedin, Utilization of 1-butylpyrrolidinium Chloride Ionic Liquid as an Eco-friendly Corrosion Inhibitor and Biocide for Oilfield Equipment: Combined Weight Loss, Electrochemical and SEM Studies Z. Phys. Chem. 235(4), 377-406 (2019). https://doi.org/10.1515/zpch-2019-1517
[70] A. M. El-Shamy, M. A. El-Hadek, A. E. Nassef, R. A. El-Bindary, Box-Behnken design to enhance the corrosion resistance of high strength steel alloy in 3.5 wt.% NaCl solution, Mor. J. Chem. 8(4), 788-800 (2020). https://doi.org/10.48317/IMIST.PRSM/morjchem-v8i4.21594